Aerodynamic Force Modeling for Unsteady Wing Maneuvers

Ryan Jantzen* and Kunihiko Taira†

Florida State University, Tallahassee, FL

Kenneth Granlund‡ and Michael V. Ol§

U.S. Air Force Research Laboratory, Wright-Patterson Air Force Base, OH

We report on the development of an aerodynamic force model for a flat-plate wing undergoing unsteady motions of surging, pitching, and the combination thereof in two-dimensional flow. This investigation aims to extend the conventional quasi-steady aerodynamic theory to account for the influence of large-scale vortices generated from the massively separated flow at high angles of attack. A data set compiled from direct numerical simulation is used to develop the force model. Particular focus is placed on examining the influence of large-amplitude wing motion on the unsteady aerodynamics force. This is especially important since the resulting circulatory component of force is significant in size and is nonlinearly related to the flow field causing deviation from conventional aerodynamic theories. The present force model is constructed to predict the aerodynamic force on the body for the duration of the wing motion.

I. Introduction

As we pursue improvement of aircraft maneuverability, the aircraft is expected to have predictable high aerodynamic performance at high angles of attack and to operate in gusty conditions. Such predictive capability is critical for unmanned air vehicles that are designed to fly in urban environment where the wake generated behind buildings and atmospheric fluctuations pose a challenge to stable flight operations. In order to achieve desirable flight performance at these conditions, it becomes necessary to develop an accurate aerodynamic force model for unsteady wing motions with large amplitudes. Compared to past quasi-steady type force theories, it is important to account for the massively separated region that forms behind wings.

The objective of the present work is to develop an unsteady force model that *requires only wing kinematics as input* to predict the normal force exerted on the wing. We note that the present study investigates large amplitude unsteady wing motions that departs from linear aerodynamic theories.[1,2] As we consider high angle of attack maneuvers, the force applied on the body is nearly normal to the surface of the wing with $L/D \approx 1$. For this reason, we select the normal force to be modeled. In this study, we limit our model to be what we refer to as the fast model. That is, we do not consider first or second-order dynamics in the model such as the one utilized by Goman and Khrabrov.[3]

In the present investigation, we base the development of the force model on the understanding gained from past studies on unsteady aerodynamics around wings undergoing various types of maneuvers. The effect of unsteady maneuvers such as pitching,[4,5,6,7,8] rotation,[9,10] surging,[11,12] and the combinations of these motions[13] have been examined. From these studies, it has been observed that the rate of motion affects the aerodynamic force significantly. It also has been observed that the decreasing aspect ratio of the wing has an effect on reducing the aerodynamic force with more influence later in time once the tip vortices develop significantly.[8] On the other hand, the change in unsteady force from varied Reynolds number can be secondary in magnitude for $Re \lesssim \mathcal{O}(10^5)$.

*Graduate Research Assistant, Department of Mechanical Engineering, rtj09@my.fsu.edu.

†Assistant Professor, Department of Mechanical Engineering, ktaira@fsu.edu.

‡Post-Doctoral Scholar, Aerospace Systems Directorate, Kenneth.Granlund.ctr@wpafb.af.mil

§Technical Advisor, Aerospace Systems Directorate, Michael.Ol@wpafb.af.mil.

Report Documentation Page

Form Approved
OMB No. 0704-0188

1. REPORT DATE	2. REPORT TYPE	3. DATES COVERED
JAN 2014		**00-00-2014 to 00-00-2014**

4. TITLE AND SUBTITLE	5a. CONTRACT NUMBER
Aerodynamic Force Modeling for Unsteady Wing Maneuvers	5b. GRANT NUMBER
	5c. PROGRAM ELEMENT NUMBER
6. AUTHOR(S)	5d. PROJECT NUMBER
	5e. TASK NUMBER
	5f. WORK UNIT NUMBER
7. PERFORMING ORGANIZATION NAME(S) AND ADDRESS(ES) **Florida State University,Department of Mechanical Engineering,Tallahassee,FL,32310**	8. PERFORMING ORGANIZATION REPORT NUMBER
9. SPONSORING/MONITORING AGENCY NAME(S) AND ADDRESS(ES)	10. SPONSOR/MONITOR'S ACRONYM(S)
	11. SPONSOR/MONITOR'S REPORT NUMBER(S)

12. DISTRIBUTION/AVAILABILITY STATEMENT
Approved for public release; distribution unlimited

13. SUPPLEMENTARY NOTES
52nd AIAA Aerospace Sciences Meeting, National Harbor, MD, Jan 13-17, 2014.

14. ABSTRACT

15. SUBJECT TERMS

16. SECURITY CLASSIFICATION OF:			17. LIMITATION OF ABSTRACT	18. NUMBER OF PAGES	19a. NAME OF RESPONSIBLE PERSON
a. REPORT	b. ABSTRACT	c. THIS PAGE			
unclassified	**unclassified**	**unclassified**	**Same as Report (SAR)**	**17**	

For this study, we limit the motion to be at a low Reynolds number of 500 (based on terminal velocity) composed of surging and pitching that is defined by the modified Eldredge function which does not introduce any discontinuity in the temporal derivatives of the motion profile. The pitching motion is taken to occur about the leading edge. The flow considered here is two-dimensional so that the effect of aspect ratio can be included later in a follow-up study. The present force model takes the wing motion as the sole input to predict the force experienced by the wing. This purpose for this choice of input is to allow for the construction of a computationally inexpensive force model that can be implemented into a vehicle control algorithm in a simple manner. In what follows, we describe the flow physics around moving wings and discuss the development of the force model, which accounts for the effects of surging, pitching, and incidence angle. A variety of motions are examined and comments are offered on the validity of the model.

II. Approach

We focus on unsteady wing motion in two-dimensional flow for a Reynolds number, $Re \equiv U_{\max} c/\nu = 500$, where $U_{\max}$ is the maximum final velocity attained by the wing at the end of the motion considered in this study. This Reynolds number is chosen to keep the flow laminar and to allow for this study to be performed in the absence of turbulence. It should be noted that the qualitative behavior of the flow field at Reynolds number below 10^5 is mostly unchanged for unsteady wing motion, which allows for this study to be applicable to higher Reynolds numbers.[8] We employ the immersed boundary projection method[14,15] to simulate the flow around the wing and the associated aerodynamic force. The immersed boundary projection method solves for the flow field on a Cartesian mesh and generates a body of arbitrary geometry with a set of Lagrangian points where boundary forces are applied to enforce the no-slip boundary condition. A typical size of the domain used in this study is $(x, y) \in [-10, 22] \times [-16, 16]$, with the leading edge of the wing position positioned at the origin. The spatial coordinates are non-dimensionalized by the chord length, c, and the temporal units are reported in terms of the convective time. The forces on the body (F_x, F_y) are non-dimensionalized using the dynamic pressure based on the final maximum translational velocity $U_{\max}$ and the chord c, defined by $C_L = F_y/\left(\frac{1}{2}\rho U_{\max}^2 c\right)$ and $C_D = F_x/\left(\frac{1}{2}\rho U_{\max}^2 c\right)$, where ρ is the density of the fluid.

III. Flow Physics

Unsteady Maneuvers

We consider the motion of surging (accelerating), pitching, and the combination thereof starting from rest. For the pitching motion, we limit our discussion to pitching about the leading edge. The effect of pitching about other pivot-points along chord of the wing are discussed in Ref. 16. The velocity and angle-of-attack profiles used for the surging and pitching motions, respectively, are defined by the modified Eldredge function[17] for a smoothed linear ramp. A linear ramp in velocity corresponds to constant acceleration and a quadratic profile for the position, whereas a linear ramp in angular position corresponds to constant angular velocity. The constant acceleration portion of the motion used in this study is similar to the motions studied by Chen et al.,[11] whose velocity profile was defined by a power law of the form $U(t) = kt^\beta$, with $\beta = 1$.

For the surging motions, the velocity profile is defined with respect to convective time ($t = Ut'/c$), given by

$$U(t) = \frac{U_{\max}}{2ac_s} \log\left[\frac{\cosh(a(t-t_1))}{\cosh(a(t-t_2))}\right] + \frac{U_{\max}}{2}, \tag{1}$$

where $U_{\max}$ is the maximum velocity the plate achieves at the end of the motion, a is a smoothing parameter for the linear-ramp profile, and $c_s = t_2 - t_1$ is the duration of the motion. Once the velocity of the plate is known, the dimensional (physical) time ($t' = ct/U$) is determined from

$$t' = c\int_0^t \frac{d\tau}{U(\tau)}. \tag{2}$$

By integrating the velocity profile, the position of the plate is determined by numerically integrating the

velocity profile:

$$s = \frac{1}{c}\int_0^{t'} U(\tau)d\tau. \tag{3}$$

Throughout this paper, we consider the position of the plate to be the convective variable of the motion. This allows for motions to be described as occurring over a certain number of chord lengths in which the flat plate has traveled. For the force modeling in the following sections, the models in consideration take the wing motion as the sole input, including the velocity of the plate and its derivatives $(\dot{s}, \ddot{s}, ...)$. The velocity of the plate as well as the higher derivatives are found by taking consecutive derivatives of the position of the plate (s) with respect to the physical time, t', i.e., $\dot{s} = ds/dt'$, $\ddot{s} = d^2s/dt'^2$, ... The position (s), velocity $(\dot{s})$, and acceleration $(\ddot{s})$ of the plate are shown plotted against convective time (t, left) and physical time (t', right) in Figure 1.

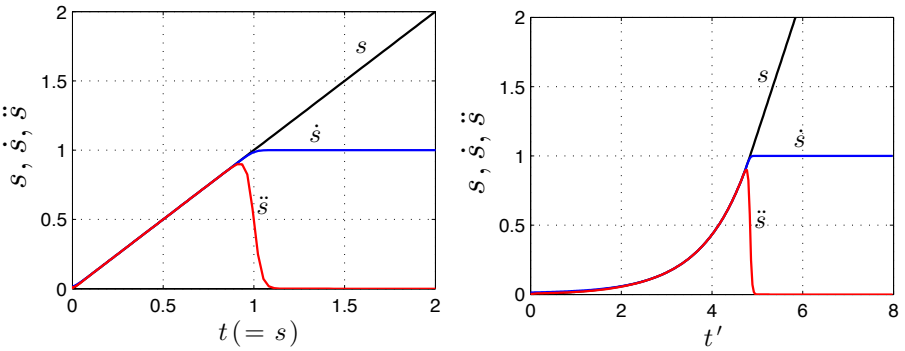

Figure 1: The position (black), velocity (blue), and acceleration (red) profiles for the surge motion plotted against convective time (t, left) and physical time (t', right). For the present motion, $c_s = t_2 - t_1 = 1$, which corresponds to a constant acceleration over one chord (c) length of travel.

For the pitching motions, the angle of attack of the flat plate with respect to convective time is given by

$$\alpha(t) = \frac{\alpha_{\max}}{2ac_p}\log\left[\frac{\cosh(a(t-t_1))}{\cosh(a(t-t_2))}\right] + \frac{\alpha_{\max}}{2}, \tag{4}$$

where $\alpha_{\max}$ is the maximum angle the plate reaches with respect to the freestream and $c_p = t_2 - t_1$ is the duration over which pitching occurs. The derivatives of the angular position which are needed for the modeling are also taken with respect to physical time, t', i.e., $\dot{\alpha} = d\alpha/dt'$, $\ddot{\alpha} = d^2\alpha/dt'^2$, ...

Vortex Dynamics

In order to understand how the aerodynamic forces are generated with unsteady plate motions, we first focus on the evolution of the vortical structures around the flat plate. Figure 2 shows the evolution of the flow field around the flat-plate wing undergoing a pure pitching (left column), combined pitch-surging (center column), and pure surging (right column) motion. The rate at which each of these maneuvers takes place is given by a reduced frequency of $K \equiv \dot{\alpha}c/2U_\infty = \alpha_{\max}c/2U_\infty c_p = \pi/8$, which corresponds to the motion taking place over 1 chord length of travel. For the pure pitching motion, the plate resides at 0° angle of attack for 10 convective units to allow for the initial transients of the simulation to die out and for the forces exerted on the plate to reach a steady value. For the pure surging motions, the plate resides in a quiescent flow at an angle of attack of $\alpha = \alpha(t_0)$ with respect to the acceleration direction. For the combined pitch-surge motion, the flat plate begins the maneuver from rest at an angle of attack of $\alpha = 0°$ with respect to the direction that the acceleration occurs. The evolution of the flow field is visualized using contours of constant spanwise vorticity given by $-25 \leq \omega_z \leq 25$.

Beginning with the pure pitching motion in the left column, the plate has a well established boundary layer at the start of the motion which rolls up and detaches at the trailing edge as the plate increases is angle of attack which then begins to advects downstream. At the leading edge of the plate, the vortex sheet rolls

	Pitch	Pitch-Surge	Surge
$t = 0.25$ $\alpha = 11°$	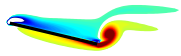	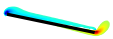	
$t = 0.50$ $\alpha = 23°$	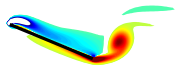	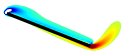	
$t = 0.75$ $\alpha = 38°$	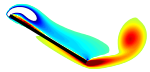	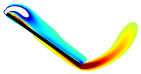	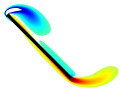
$t = 1.00$ $\alpha = 45°$	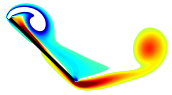	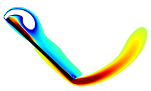	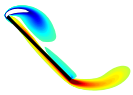
$t = 1.50$ $\alpha = 45°$	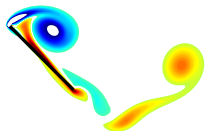	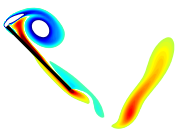	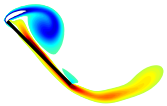
$t = 2.00$ $\alpha = 45°$	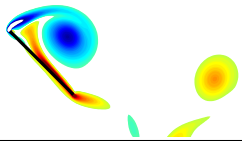	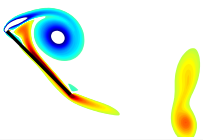	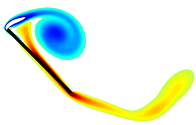

Figure 2: Evolution of the flow field around a flat-plate wing undergoing a pure pitching (left column), combined pitch-surging (center column), and pure surging (right column) motion at a reduced frequency of $K = \pi/8$ and $Re = 500$. The flow around these plates is visualized using contours of $-25 \leq \omega_z \leq 25$.

up into a compact leading-edge vortex (LEV) that presents a low pressure region on the top surface of the wing. This low pressure region enhances the lift of the plate as it continues to increase its angle of attack. By the end of the motion ($t \geq 1$), the plate is at an angle of $\alpha_{\max} = 45°$ and the LEV continues to grow over the surface of the wing.

Unlike the pure pitching motion, there is no well established boundary layer at the start of the motion for the surge and combined pitch-surge maneuver since the motion of the plate begins from rest. This results in the absence of trailing edge vortices for both the pure sure motion and the combined pitch-surge motion. For the pure surge motion, the flow detaches from the leading edge at the beginning of the motion due to the plate's high angle of attack of $\alpha_{\max} = 45°$. This results in a relatively weak LEV that forms during the motion, which is seen to be smeared along the chord of the wing when compared to the LEV that develops for both the pure pitching and combined pitch-surge motions. For the pitch-surge motion, the plate begins to accelerate from $\alpha = 0°$, which results in the flow being attached during the early potion of the motion. As the plate continues to accelerate and increase its angle of attack, the flow field resembles that of the pure pitching motion. By the end of the motion, the LEV appears to be more compact and located closer to the wing surface with a greater strength compared to the LEV that develops for the pure pitching case, which is due to the increased circulation due to the combined motion, and enhances the lift force.

Aerodynamic Forces

The temporal evolution of the lift and drag coefficients for the three motions under consideration is given in Figure 3 for both the present simulations ($Re = 500$, solid curve) and companion experimental measurements performed in a horizontal water tunnel at the Air Force Research Laboratory at Wright-Patterson Air Force Base[16]($Re = 20,000$, dashed curve). As the plate begins to increase its angle of attack for the pure pitching motion, a large spike in the lift coefficient is observed, which results from the initial angular acceleration of the plate. As the plate continues to increase its angle of attack, the lift force begins to rise again due to the development of the LEV over the top surface of the wing. At the end of the motion, a negative spike in the lift coefficient is observed due to the angular deceleration of the plate.

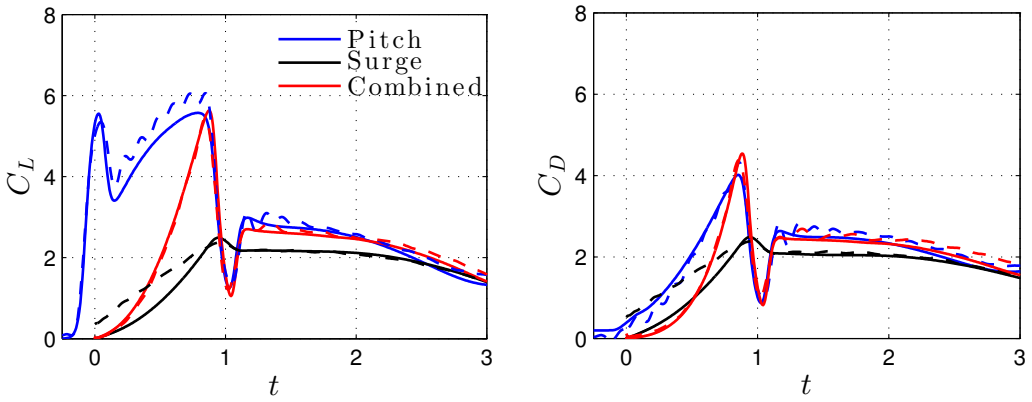

Figure 3: Comparison between the experimental ($Re = 20,000$, dashed) and present simulation ($Re = 500$, solid) force coefficients for a flat plate wing undergoing a pitching (red curve), surging (black curve), and a combined pitch-surge motion (blue curve) at a reduced frequency of $K = \pi/8$, which corresponds to occurring over one chord length of travel.

For the pure surging and combined pitch-surge maneuvers, the forces are initially zero since the plates start from rest. As the motion begins, the lift and drag coefficients begin to increase. This increase is much more rapid for the combined motion due to the very tight, compact LEV that forms above the wing. Towards the end of the maneuver, the lift coefficient for the combined motion is nearly three times that of the pure surging motion. Although the initial evolutions of the lift and drag coefficients for these three motions are vastly different, both lift and drag forces on the plate collapse for the three maneuvers roughly 2 convective units after the completion of the motion.

Similar trends between the lift and drag coefficients for both Reynolds numbers considered are observed. Although there is two orders of magnitude difference in the Reynolds number between the present simulations and the experiments, we observe agreement between the forces generated for these high-amplitude maneuvers.

This observation gives us confidence that the force modeling performed in the following sections for the present low-Reynolds number maneuvers can be extended to higher Reynolds number flows.

IV. Force Model

Pure Surge Motion

First, let us consider the wing at a constant angle of attack of $\alpha = 45^\circ$ accelerating from rest. The wing will accelerate linearly over c_s convective units before reaching a constant velocity $U_{\max}$. Based on prior research on unsteady flows around moving wings, we have observed that the normal force is the dominant force acting on the wing. In fact for most conditions considered in this study, the lift to drag ratio is approximately one. For this reason, we will model the normal force on the wing in the present study for all motion profiles considered.

In order to capture the normal force, we have considered various functional forms based on the kinematics and observed that the following expression approximates the normal force well:

$$F_N \approx c_1 \dot{s}(\sqrt{\dot{s}} + \ddot{s}), \tag{5}$$

where c_1 is a constant to be selected and the dot represents the time derivative. The right hand side of this equation is found to perform fairly well for a wide range of acceleration. Based on this observation, we have generalized the force model to be

$$F_N \approx c_1 \dot{s}^{\beta_1} + c_2 \dot{s}^{\beta_2} \ddot{s}. \tag{6}$$

We test this model for $1 \leq c_s \leq 8$ and tune the parameters c_1, c_2, β_1, and β_2 for each value of c_s using a least-squares fit. The comparison of the DNS data and the force model that is tuned for each case is shown in Figure 4. It can be seen that when the optimal model coefficients are used, the model predicts the force so well that they are almost indistinguishable during acceleration. The error during acceleration is limited to less than 5% of the maximum normal force during the time interval of interest. While comparing the forces, we have found that the comparison of the maximum force value is an effective indicator to evaluate the accuracy of the force models. In what follows, we present the comparison of the force model with the DNS results along with the maximum force values and the errors.

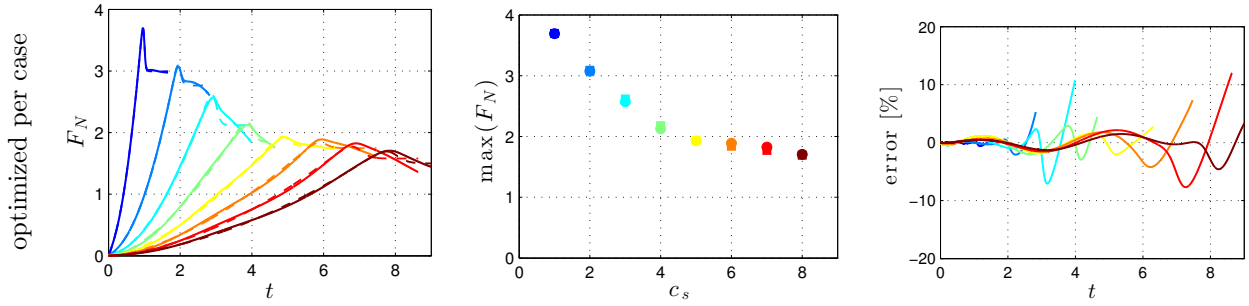

Figure 4: The force model based on Eq. (6) with its coefficients tuned for each surging case is compared with the DNS results. The left figure compares the force model (dashed) against the DNS results (solid). The center plot compares the maximum normal force for each of the surging case (circle = DNS and square = model). The right plot is the error between the model and the DNS results normalized by the maximum force over the time interval considered.

While the model in Figure 4 predicts the DNS forces quite well, it would be more desirable to find the force model that does not require fitting of the model coefficients for each and every case. In order to find the trend associated with the effect of acceleration on the normal force and its model, let us curve fit the model for a selected surging case and use the selected model parameters (c_1, c_2, β_1, and β_2) for all other surging cases. We show the comparison made for models tuned at $c_s = 2, 4$, and 8 in Figure 5. It can be noticed that the model tuned for faster surge rates do not predict the slower surge rate cases well. The large difference can be seen at higher c_s for the model tuned at $c_s = 2$. However, the model tuned for slower surge rates predicts the faster surge rate cases well. These observations suggest that some of the model parameters need to be carefully tuned to predict the normal force accurately.

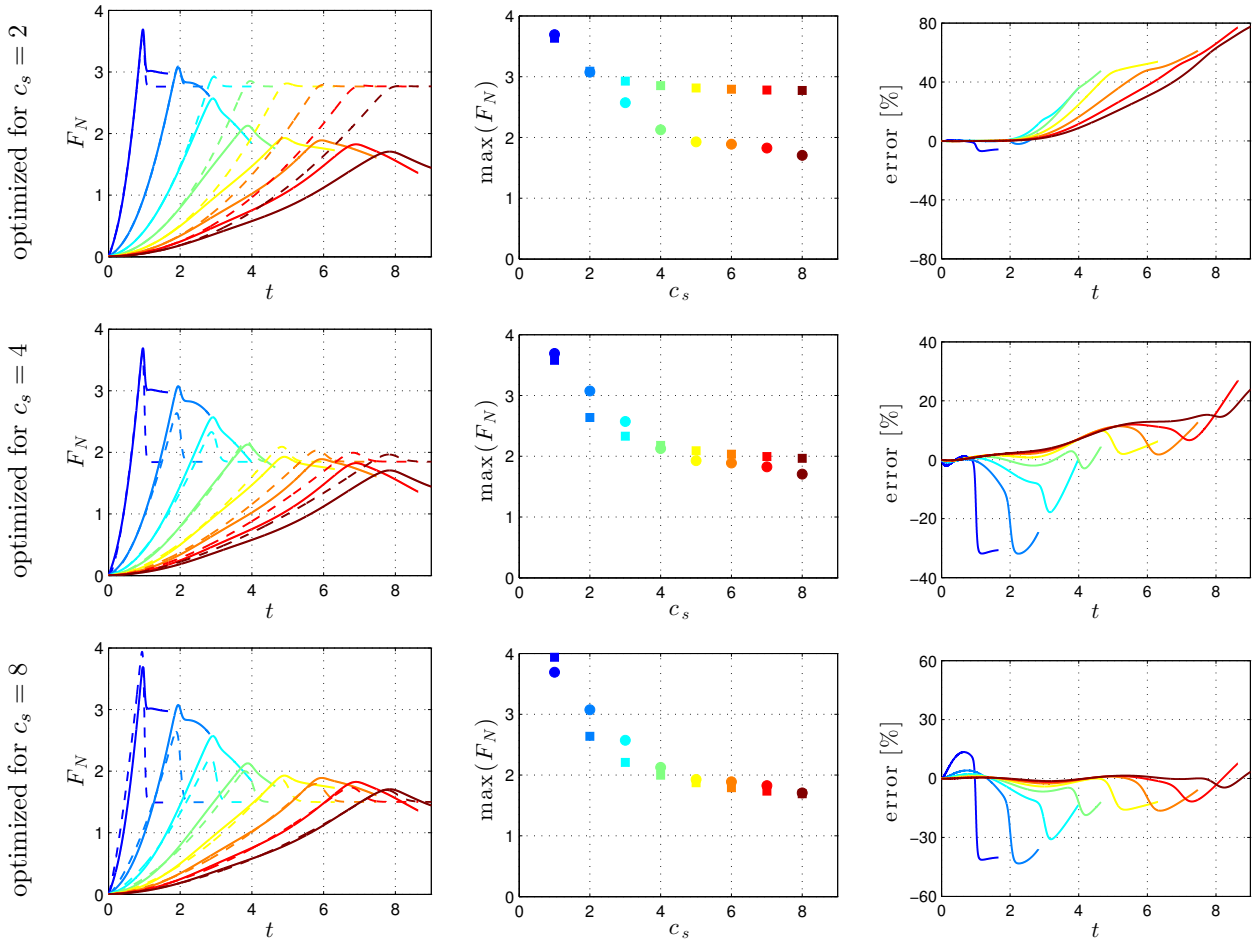

Figure 5: The force model based on Eq. (6) with its coefficients tuned only for the indicated surging case is compared with the DNS results. See Figure 4 for legends and symbols.

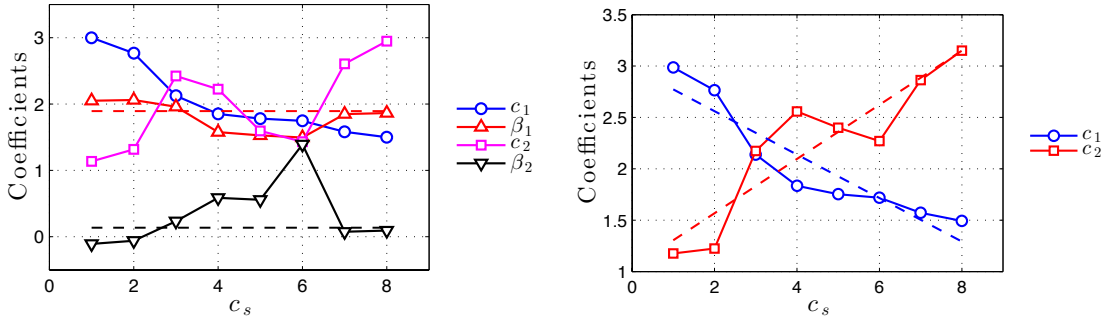

Figure 6: The variation in the exponents β_1 and β_2 and the coefficients c_1 and c_2 (left). The variation in coefficients c_1 and c_2 with fixed exponents (right). Shown are the linear approximations for c_1 and c_2.

The behavior of the model parameters tuned for each surge rate case is presented in Figure 6. Except for the results for $c_s = 6$, the values of the exponents β_1 and β_2 do not vary significantly. Hence, we approximate the exponents with their average values

$$\beta_1 \to \text{avg}\beta_1 = 1.89 \quad \text{and} \quad \beta_2 \to \text{avg}\beta_2 = 0.138. \tag{7}$$

For the coefficients in front of the force model terms, it is possible to use the mean values following the approach taken for the exponents:

$$c_1 \to \text{avg}c_1 = 2.03 \quad \text{and} \quad c_2 \to \text{avg}c_2 = 2.23. \tag{8}$$

We can also consider the coefficients c_1 and c_2 to be linearly related to c_s, as shown in Figure 6. The linear approximations for c_1 and c_2 are

$$c_1 \to -0.212c_s + 2.98 \quad \text{and} \quad c_2 \to 0.2636c_s + 1.04. \tag{9}$$

These coefficients are shown with the exponents β_1 and β_2 fixed to the mean values.

Next, let us compare the force model performance based on the choices proposed above. In Figure 7, we compare the models based on

(i) coefficients tuned for the surge case with $c_s = 4$,
(ii) using mean values for all exponents and coefficients (using Eqs. (7) and (8)), and
(iii) using the mean exponents and linear model for the coefficients (based on Eqs. (7) and (9))

Of the three models considered here and shown in Figure 7, we find that setting the exponents to be the mean values and linearly approximating the coefficients accurately predicts the unsteady force on a wing undergoing surging motion. Thus, we use the last force model in what follows. To summarize, the unsteady normal force model for the surging case is

$$\begin{aligned} &\text{(pure surge)} \quad F_N \approx c_1 \dot{s}^{\beta_1} + c_2 \dot{s}^{\beta_2} \ddot{s}, \\ &\qquad\qquad \text{where} \quad \alpha_1 = 1.89, \ \alpha_2 = 0.138, \\ &\qquad\qquad\qquad\quad c_1 = -0.212c_s + 2.98, \ c_2 = 0.2636c_s + 1.04. \end{aligned} \tag{10}$$

Variation in the Angle of Attack

For the above model, we have only considered the case of the wing being at an angle of attack of 45°. In order to have the normal force prediction be applicable to any angle of attack, we pre-multiply the above normal force model by a factor of $\sin(\alpha)/\sqrt{2}$ so that the model intersects the results at 45°. This also ensures that the normal force becomes zero at $\alpha = 0°$ and achieves the maximum value at 90°, respectively. The

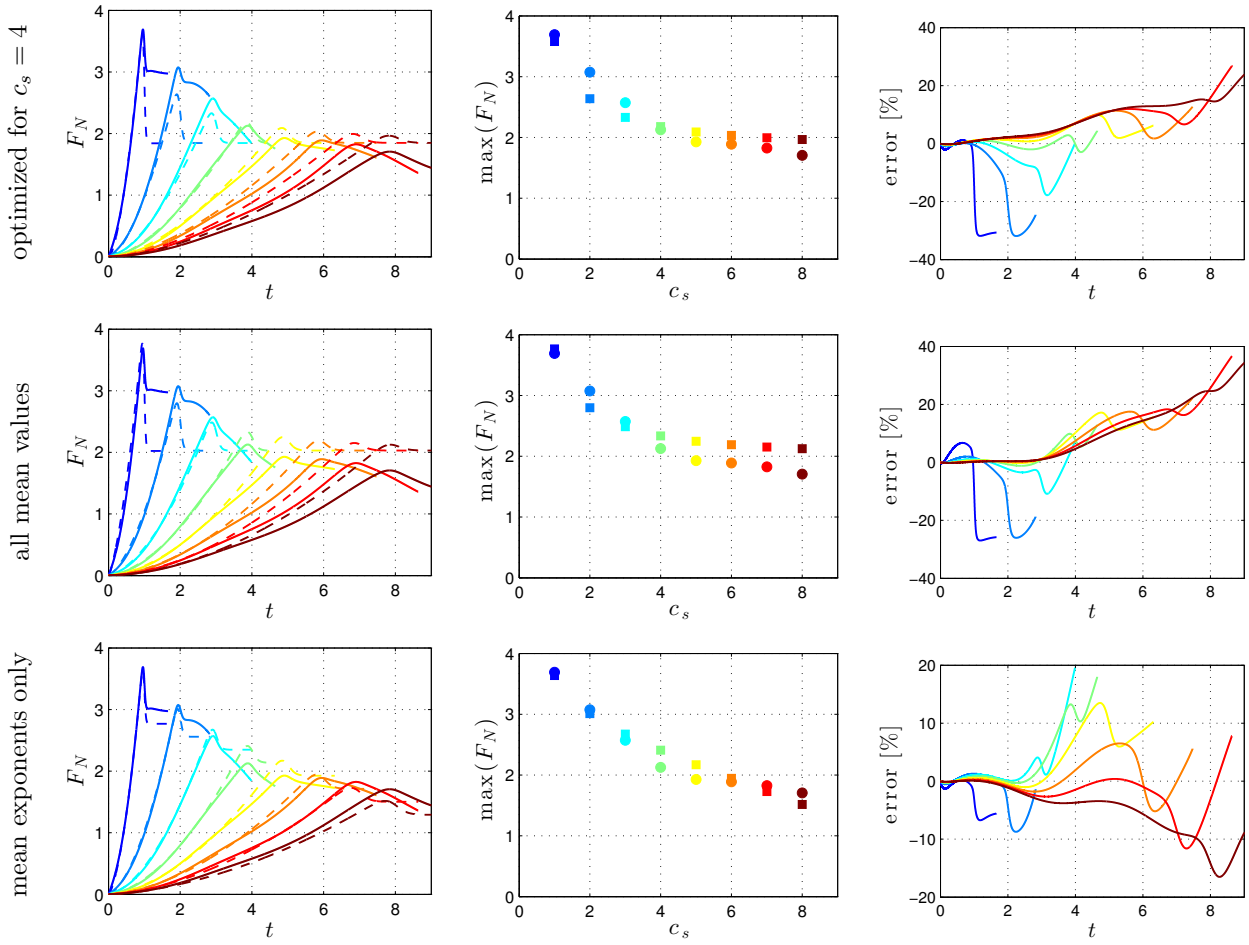

Figure 7: Summary of the model comparison. Shown are the models (top) tuned for $c_s = 4$, (middle) using mean values for all coefficients, and (bottom) only fixing the exponents with mean values. See Figure 4 for legends and symbols.

overall results for the example of $c_s = 4$ for various angles of attack are presented in Figure 8. It can be seen that this simple scaling captures the normal force well for a wide range of incidence angles:

$$\boxed{\begin{aligned}&(\text{surge for } 0 \le \alpha \le 90^\circ) \quad F_N \approx \frac{1}{\sqrt{2}} \sin(\alpha) \left[c_1 \dot{s}^{\beta_1} + c_2 \dot{s}^{\beta_2} \ddot{s} \right], \\ &\qquad\qquad \text{where} \quad \beta_1 = 1.89, \ \beta_2 = 0.138, \\ &\qquad\qquad\qquad\quad c_1 = -0.212 c_s + 2.98, \ c_2 = 0.2636 c_s + 1.04.\end{aligned}} \tag{11}$$

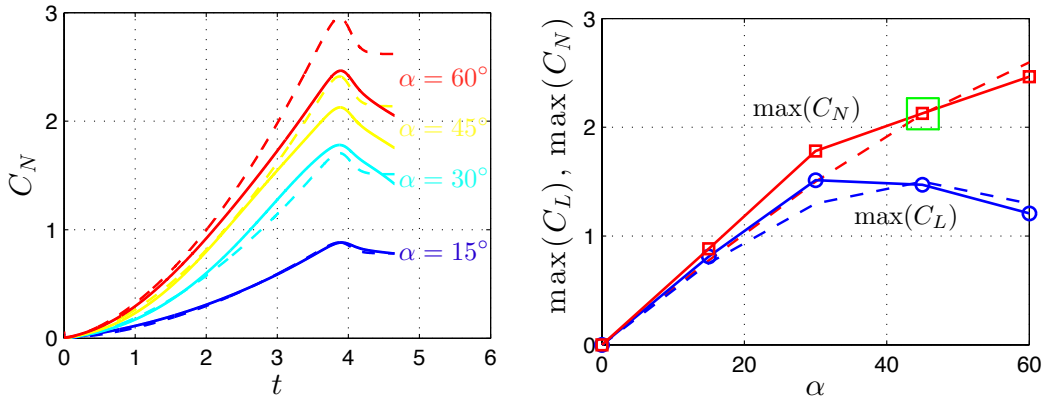

Figure 8: The surging case results shown for $\alpha = 15°$, $30°$, $45°$, and $60°$.

Extension to Pitch-Surge Motions

Next, we extend the above force model for surging to a combined pitch-surge motion initiating from rest. We first consider the surge and pitching motions to take place at the same reduced frequency and generalize it for motions with different rates. The proposed force model expressed by Eq. (11) includes the influence of the angle of attack α. Since the first and second time derivatives of the incidence angle is not included in this model, we do not expect to accurately predict the unsteady force especially for faster maneuvers where quasi-steady assumptions do not hold. This can be seen from Figure 9, where the normal force from fast motion exhibit large difference from the force predicted by Eq. (11).

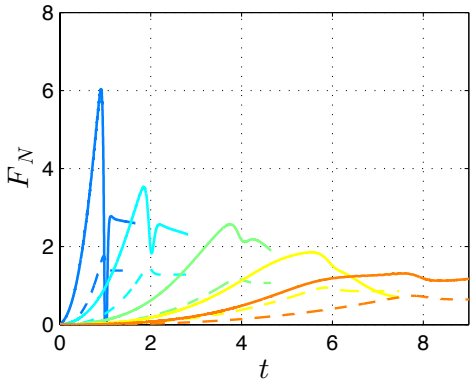

Figure 9: Naive application of Eq. (11) to combined pitch-surge motion cases (solid lines: DNS, dashed lines: model).

In order to account for the difference between the aforementioned force model, Eq. (11), and the forces generated by the pitching motion, we utilize the insights obtained from research on pure pitching cases.[16,18] That is, we add the unsteady forces that are proportional to $\dot{\alpha}$ and $\ddot{\alpha}$. Hence, for the pitch-surge force model,

we arrive at

$$F_N \approx \frac{1}{\sqrt{2}} \sin(\alpha) \left[c_1 \dot{s}^{\beta_1} + c_2 \dot{s}^{\beta_2} \ddot{s} \right] + d_1 \dot{\alpha} \dot{s}^2 + d_2 \ddot{\alpha} \dot{s}^2, \tag{12}$$

where two coefficients d_1 and d_2 need to be empirically determined. In Figure 10, we present the above model with d_1 and d_2 based on the DNS results. The other coefficients and exponents are held fixed from the pure surging cases. This proposed pitch-surge model tuned for each case considered in Figure 10 agrees well with the normal force obtained from simulation. We can also observe that coefficients d_1 and d_2 can be approximated by a linear function and the mean value, respectively. With such simplification, we arrive at the final version of the combined pitch-surge force model of

$$\begin{aligned} &\text{(pitch-surge)} \quad F_N \approx \frac{1}{\sqrt{2}} \sin(\alpha) \left[c_1 \dot{s}^{\beta_1} + c_2 \dot{s}^{\beta_2} \ddot{s} \right] + d_1 \dot{\alpha} \dot{s}^2 + d_2 \ddot{\alpha} \dot{s}^2, \\ &\text{where} \quad \beta_1 = 1.89, \ \beta_2 = 0.138, \\ &\qquad\quad c_1 = -0.212 c_s + 2.98, \ c_2 = 0.2636 c_s + 1.04, \\ &\qquad\quad d_1 = 0.834 c_p + 7.61, \ d_2 = 0.582. \end{aligned} \tag{13}$$

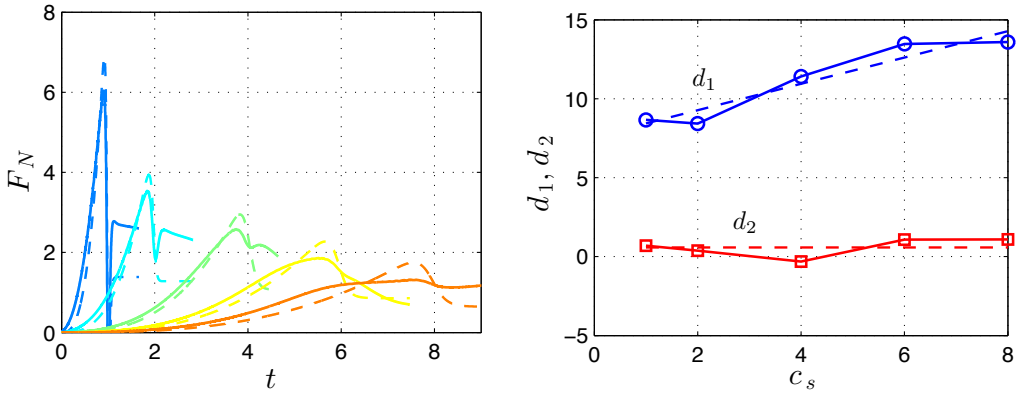

Figure 10: The normal force prediction on the left (solid: DNS and dashed: model) made by the combined pitch-surge model of Eq. (12) where the coefficients d_1 and d_2 are tuned for each case, as shown on the right.

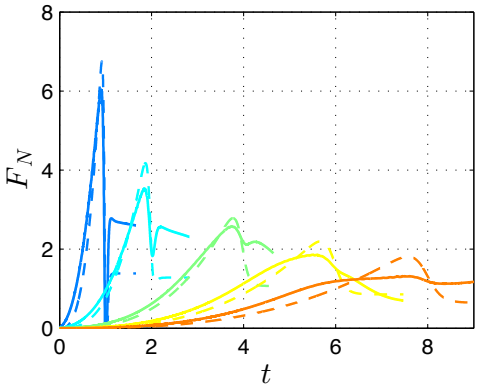

Figure 11: The normal force prediction based on the combined pitch-surge model, Eq. (13), with the coefficients given by mean values and linear function of c_a (solid: DNS and dashed: model).

This final form of the model captures the normal force on a wing accurately for a wide range of pitch/surge rates, as shown in Figure 11. Note that the rates shown in this figure ($c_s = c_p = 1, 2, 4, 6, 8$) span across the rate corresponding to the universal formal time of vortices.[19] Hence it can be seen that this proposed model

can approximate the force very well, not only during the wake vortex formation but also after the creation of the maximally grown wake vortex.

In order to assess how the model performs for more general motions, we will now compare the present model to simulations for combined pitch-surge motions where the pitch and surge rates are different. Figure 12 shows the results for the combined pitch-surge motions over a range of pitch($c_p = 1, 4$, and 6) and surge rates ($c_s = 1, 4$, and 6). The vertical lines in the plots highlight regions where the pitching motion (- - - -) and surging motion (— - —) are completed. The opaque portion of the plots indicate regions after the wing motion has completed for which the force model is not designed to predict. The deviation in force after the wing maneuver results from the fact that the only input to the model is the wing kinematics. In some cases, however, it is observed that after the motion has finished the model continues to predict the force on the plate reasonably well. This is primarily due to the inherent dynamics of the LEV formation that is embedded within the coefficients, which were empirically determined to match the DNS results.

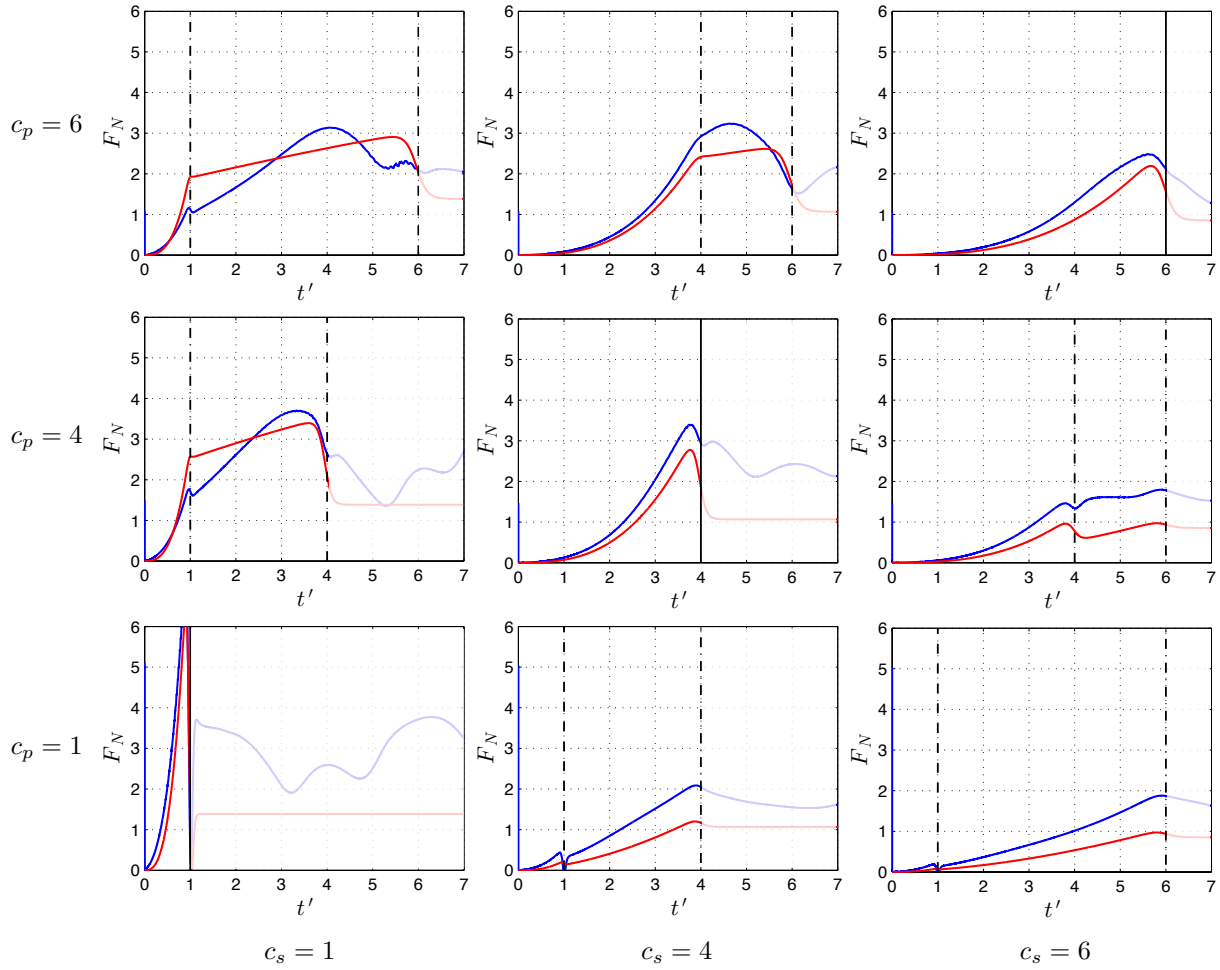

Figure 12: The normal force prediction based on the combined pitch-surge model, Eq. (13), for maneuvers in which the pitch-rate and surge-rate are different. The vertical lines correspond to the end of the pitching motion (- - - -), the end of the surging motion (— - —), and the end of both motions when the rates are the same (———). The opaque regions of the plots are regions where the model is not designed to predict the unsteady force exerted on the plate.

Along the diagonal of Figure 12 where the pitch-rate matches the surge-rate ($c_p = c_s$), the model captures the increase of the force but slightly under predicts the peak normal force at the end of the motion. For the cases where the pitch-rate is greater than the surge-rate ($c_p < c_s$), the model predicts the similar trend of how the force increase but under predicts the peak force at the end of the motion. Finally, for the cases in which the surge-rate is greater than the pitch-rate ($c_p > c_s$), the model shows more deviation from the actual forces determined by the DNS. When the plates translational acceleration is faster than the rotational acceleration, a quick drop in the normal force is observed before the motion has completed. This sudden

drop is due to the development of the LEV over the plate. These trends are somewhat predicted as the present force model is originally derived for cases with the pitch and surge rates matching. Even with the observed difference off the diagonal of Figure 12, we note that the current predictions are reasonable as the motion amplitudes are large with high frequency components in most cases.

V. Comparison with Wagner's Theory

In order to assess the validity for the force model developed in the present study, the forces predicted in the previous sections are now compared to Wagner's inviscid theory for unsteady airfoils at small angles of attack. Chen et al.[11] and Pullin and Wang[20] have used this model as a validation for accelerating flat plates and ellipses', respectively. For surging motions with constant acceleration, Wagner's theory predicts the forces in the x and y directions for small s and α as:

$$F_{x'} = \frac{d}{dt}(m'_{11}U(t)) \tag{14}$$

$$F_{y'} = \frac{\pi}{2}\rho c U^2(t)\sin(\alpha) + \frac{d}{dt}(m'_{21}U(t)) \tag{15}$$

In the previous two equations, the primed coordinates, (x', y'), are in the direction of the maneuvering wing, rotated from the body fitted coordinates, (x, y), and m'_{ij} is the added mass tensor in these rotated coordinates ($\mathbf{m'} = \mathbf{RmR}^{-1}$), where $\mathbf{m}$ is the added mass tensor in the body fitted coordinates and $\mathbf{R}$ is the rotation matrix between the body fitted coordinates and the primed coordinates, both given by

$$\mathbf{m} = \begin{pmatrix} -\pi\rho b^2 & 0 \\ 0 & -\pi\rho a^2 \end{pmatrix} \tag{16}$$

and

$$\mathbf{R} = \begin{pmatrix} \cos(\alpha) & -\sin(\alpha) \\ \sin(\alpha) & \cos(\alpha) \end{pmatrix}. \tag{17}$$

For the pure surging motions, the terms dependent on α in the added mass tensor are independent of time ($\dot{\alpha} = 0$), therefore Wagner's theory predicts the forces in the (x', y') direction as

$$F_{x'} = \frac{\pi}{2}\rho c^2 \sin^2(\alpha)\frac{dU}{dt} \tag{18}$$

$$F_{y'} = \frac{\pi}{2}\rho c U^2 \sin(\alpha) + \frac{\pi}{2}\rho c^2 \cos(\alpha)\sin(\alpha)\frac{dU}{dt} \tag{19}$$

For the combined maneuvers that include both surging and pitching motions, the angle of attack is time dependent ($\alpha = \alpha(t)$), thus the derivatives of the added mass tensor must be evaluated, and the resulting forces in the (x', y') direction are given by

$$F_{x'} = \frac{\pi}{2}\rho c^2 \left[2\cos(\alpha)\sin(\alpha)\frac{d\alpha}{dt}U(t) + \sin^2(\alpha)\frac{dU}{dt}\right] \tag{20}$$

$$F_{y'} = \frac{\pi}{2}\rho c U^2 \sin(\alpha) + \frac{\pi}{2}\rho c^2 \left[(\cos^2(\alpha) - \sin^2(\alpha))\frac{d\alpha}{dt}U(t) + \cos(\alpha)\sin(\alpha)\frac{dU}{dt}\right] \tag{21}$$

In the analysis to follow, the forces predicted by Wagner's inviscid theory are presented as the normal force to be consistent with the previous analysis.

We first consider the comparison between the numerical simulations, the present force modeling results, and the theory of Wagner for the pure surging case, as seen in Figure 13. For this comparison, we consider the cases of constant acceleration over $1, 2, 4$, and 6 chord lengths of travel $c_s = 1, 2, 4, 6$ at an angle of $\alpha = 45°$. For the two fastest cases considered ($c_s = 1$ and 2), the present model predicts the normal force

very well throughout the acceleration as well as the peak normal force at the end of the motion. For the two slower cases, the model begins to deviate towards the end of the acceleration, which could be due to the slow dynamics associated with the development of the LEV over the wing. It can be seen that Wagner's model under predicts the normal force for all of the motions considered, which was expected due to the absence of the LEV formation in the model.

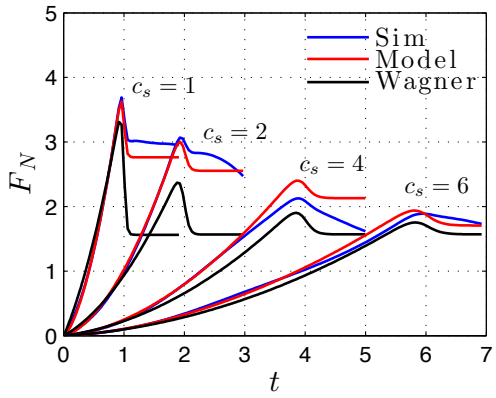

Figure 13: Comparison of the computational results, the present force model, and the theory of Wagner for the pure surging motion of constant acceleration over $1, 2, 4$, and 6 chord lengths of travel at $Re = 500$ and $\alpha = 45°$.

Next, we assess the results for the pure surging case with a variation in angle of attack by comparing the simulations, present force model, and the theory of Wagner, as seen in Figure 14. The constant acceleration for the present comparison occurs over 1 chord length of travel ($c_s = 1$) and the variation in angle of attack is between $\alpha = 15°, 30°, 45°$ and $60°$. The present force model predicts the normal force throughout the accelerated portion for this fast motion very well over all angles of attack considered. After the acceleration has ended, there is no drop in the force that is predicted with the present model when compared to Wagner's model. It can be seen that for the smallest angle considered ($\alpha = 15°$), Wagner's theory predicts the normal force very well though the constant accelerated motion due to the satisfying the small angle assumption over short travel distances, in which a large LEV is not observed.

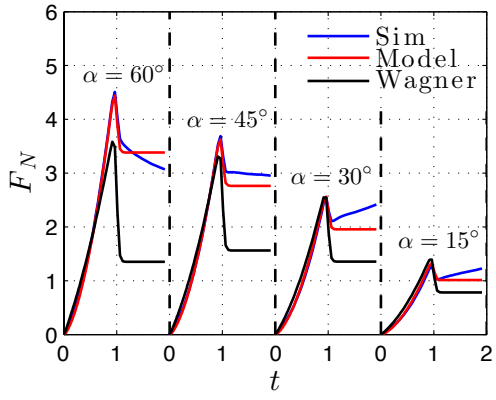

Figure 14: Comparison of the computational results, the present force model, and the theory of Wagner for the pure surging motion of constant acceleration over 1 chord length of travel and a variation of angle of attack for $\alpha = 15°, 30°, 45°$ and $60°$.

We now compare the present force model for the combined pitch and surge motion with the simulations and the theory of Wagner, as seen in Figure 15. The combined motion for the present comparison occurs over $1, 2, 4$, and 6 chord lengths of travel ($c_s = c_p = 1, 2, 4$, and 6, respectively) and the flat plate pitches from $\alpha = 0°$ to $\alpha_{\max} = 45°$. For these combined motions, the present model predicts the development of the normal force on the flat plate for these complex maneuvers relatively well for the two fastest motions, but under predicts the peak force at the end of the motion. It can also be seen that after the motion has

finished, the normal force drops has been previously observed for Wagner's model for the pure surging cases. Although the present model does under predict the normal force for these motions, it still reasonably predicts the forces compared to the Wagner's model.

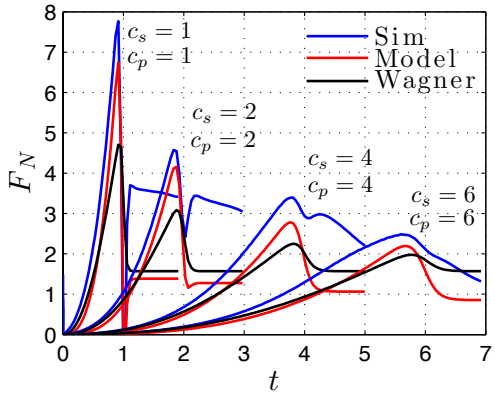

Figure 15: Comparison of the computational results, the present force model, and the theory of Wagner for the combined pitch-surge motion occurring over 1, 2, 4, and 6 chord lengths of travel ($c_s = c_p = 1, 2, 4$, and 6, respectively) at $Re = 500$. The pitching motion for the present results is from $\alpha = 0°$ to $\alpha_{\max} = 45°$.

VI. Discussion on the Force Model

Let us further comment on the final form of the present unsteady nonlinear force model. We note that the model is comprised of mainly three components, namely the parts that capture surging, pitching, and incident angle effects, as shown below:

$$F_N \approx \underbrace{\frac{1}{\sqrt{2}}\sin\alpha}_{\text{incidence angle}} \underbrace{[c_1\dot{s}^{\beta_1} + c_2\dot{s}^{\beta_2}\ddot{s}]}_{\text{surging}} + \underbrace{d_1\dot{\alpha}\dot{s}^2 + d_2\ddot{\alpha}\dot{s}^2}_{\text{pitching}}. \tag{22}$$

We can non-dimensionalize the above normal force with instantaneous velocity $\dot{s}$

$$C_N = \frac{F_N}{\frac{1}{2}\rho_\infty \dot{s}^2 c} \approx \sqrt{2}\sin\alpha[c_1\dot{s}^{\beta_1-2} + c_2\dot{s}^{\beta_2-2}\ddot{s}] + 2d_1\dot{\alpha} + 2d_2\ddot{\alpha}, \tag{23}$$

where we have taken ρ_∞ and c to be unity without the loss of generality.

Next, let us compare our model with other linear aerodynamic force models. For a wing at fixed low angle of attack with steady motion (in absence of pitching), we find that $\sin\alpha \approx \alpha$ and the above expression becomes

$$C_N \approx \sqrt{2}c_1\dot{s}^{\beta_1-2}\alpha = 4.21\dot{s}^{0.11}\alpha \approx 4.21\alpha = 0.67(2\pi)\alpha, \tag{24}$$

which tells us that the present model estimates the steady lift slope $a_0 = dC_l/d\alpha$ to be 0.67% of the potential value (2π). This is in agreement with the numerical finding from Taira and Colonius[21] that reports the lift close at low α to be $a_0 = 0.73(2\pi)$. The lower lift slope compared to the potential value is due to the viscous effects at the low Reynolds number selected here. For higher Reynolds number, c_1 can be replaced with a larger value to take Reynolds number effect into consideration (i.e. $c_1 = c_1(Re)$).

We also note that for small $\ddot{s}$ and α, the pitch-surge model reduces to

$$C_N \approx \sqrt{2}c_1(k_s)\alpha + 2d_1(k_p)\dot{\alpha} + 2d_2\ddot{\alpha}, \tag{25}$$

where dependence on pitch and surge-based reduced frequencies k_p and k_s, respectively, are shown if present. It can be noticed that this form of the equation shares similarity with Theodorsen's model[1]

$$C_{L,\text{Theodorsen}} = 2\pi C(k)\alpha + \left[\frac{\pi}{4} + \frac{3\pi}{2}\frac{c}{U_\infty}C(k)\right]\dot{\alpha} + \frac{\pi}{4}\frac{c}{U_\infty}\ddot{\alpha}, \tag{26}$$

where $C(k)$ is the Theodorsen's function.[2]

In upcoming studies, we will incorporate the effect of aspect ratio using the a relationship similar to the one proposed by Helmbold[22]

$$C_{L,3D} = \frac{C_{L,2D}}{\sqrt{1 + (2/AR)^2} + 2/AR}. \tag{27}$$

into the unsteady model developed for the two-dimensional wing.

VII. Summary

An nonlinear aerodynamics force model is developed for wings undergoing large-amplitude unsteady maneuvers. The motion considered includes surging, pitching, and the combination of the two for low Reynolds number two-dimensional flow. The proposed model is able to accurately predict normal force on the wing based on two-dimensional DNS results over a range of motion profiles and angles of attack. One advantage of the present model is that the input is only the wing kinematics and does not require any knowledge of vortex dynamics. For this reason, the normal force can be predicted with practically no computational expense. What remains to be completed with this research effort is to further test the proposed model for a wider variety of wing motion and higher Reynolds number flows. Since knowledge from past research[16,18] suggests that force on the wing is fairly Reynolds number independent for flow below transition ($Re \lesssim 10^5$), we expect the present force model to be applicable to cases with higher Reynolds numbers.

Acknowledgments

RJ and KT were supported by the 2013 ASEE Summer Faculty Fellowship Program at the Wright–Patterson Air Force Base.

References

[1]Theodorsen, T., "General theory of aerodynamic instability and the mechanism of flutter," Tech. Rep. 496, NACA, 1935.

[2]Leishman, G., *Principles of helicopter aerodynamics*, Cambridge Univ. Press, 2nd ed., 2006.

[3]Goman, M. and Khrabrov, A., "State-space representation of aerodynamic characteristics of an aircraft at high angles of attack," *J. Aircraft*, Vol. 31, No. 5, 1994, pp. 1109–1115.

[4]Buchholz, J. H. J. and Smits, A. J., "On the evolution of the wake structure produced by a low aspect ratio pitching panel," *J. Fluid Mech.*, Vol. 546, 2006, pp. 433–443.

[5]Green, M. A., Rowley, C. W., and Smits, A. J., "Thr unsteady three-dimensional wake produced by a trapezoidal panel." *J. Fluid Mech.*, Vol. 685, 2011, pp. 117–145.

[6]Garmann, D. J. and Visbal, M. R., "Numerical investigation of transitional flow over a rapidly pitching plate," *Phys. Fluids*, Vol. 23, 2011, pp. 094106.

[7]Granlund, K., OL, M., and Bernal, L. P., "Unsteady pitching flat plates," *J. Fluid Mech.*, Vol. 733, 2013.

[8]Jantzen, R., Taira, K., Granlund, K., and Ol, M., "Unsteady Vortex Dynamics of Pitching Plate Wakes," *Phys. Fluids*, In preparation.

[9]Garmann, D. J., Visbal, M. R., and Orkwis, P. D., "Three-dimensional flow structure and aerodynamic loading on a revolving wing." *PF*, Vol. 25, No. 3, 2013.

[10]Jones, A. and Babinsky, H., "Unsteady lift generation on rotating wings wings at low Reynolds numbers." *JA*, Vol. 47, 2010, pp. 1013–1021.

[11]Chen, K. K., Colonius, T., and Taira, K., "The leading-edge vortex and quasisteady vortex shedding on an accelerating plate," *PF*, Vol. 22, 2010.

[12]Ford, C. W. P., Stevens, R., and Babinsky, H., "Flexible leading edge flap on an impulsively started flat plate at low Reynolds numbers." AIAA Paper 2012-2840, 2012.

[13]Stevens, R., Ford, C. W. P., and Babinsky, H., "Experimental studies of an accelerating, pitching, flat plate at low Reynolds numbers." AIAA 2013-0677, 2013.

[14]Taira, K. and Colonius, T., "The immersed boundary method: a projection approach," *J. Comput. Phys.*, Vol. 225, 2007, pp. 2118–2137.

[15]Colonius, T. and Taira, K., "A fast immersed boundary method using a nullspace approach and multi-domain far-field boundary conditions," *Comput. Methods Appl. Mech. Engrg.*, Vol. 197, 2008, pp. 2131–2146.

[16]Granlund, K., Ol, M., Taira, K., and Jantzen, R., "Parameter Studies on Rotational and Translational Accelerations of Flat Plates," 51st AIAA ASM meeting (AIAA2013-0068), 2013.

[17]Eldredge, J. D., Wang, C., and Ol, M. V., "A Computational Study of a Canonical Pitch-up, Pitch-down Wing Maneuver," 39th AIAA Fluid Dynamics Conference (AIAA2009-3687), 2009.

[18]Jantzen, R., Taira, K., Granlund, K., and Ol, M., "On the influence of pitching and acceleration on vortex dynamics around a low-aspect-ratio rectangular wing," 51st AIAA ASM meeting (AIAA2013-0833), 2013.

[19]Gharib, M., Rambod, E., and Shariff, K., "A universal time scale for vortex ring formation," *J. Fluid Mech.*, Vol. 360, 1998, pp. 121–140.

[20]Pullin, D. I. and Wang, Z. J., "Unsteady forces on an accelerting plate and application to hovering insect flight," *J. Fluid Mech.*, Vol. 509, 2004, pp. 1–21.

[21]Taira, K. and Colonius, T., "Three-dimensional flows around low-aspect-ratio flat-plate wings at low Reynolds numbers," *J. Fluid Mech.*, Vol. 623, 2009, pp. 187–207.

[22]Helmbold, H. B., "Der unverwundene ellipsenflugel als tragende flanche," *Jahrbuch 1942 der Deutch Luftfahrtforsch*, 1942, pp. 111–113.